THE ASTROPHYSICAL JOURNAL, 544:903–920, 2000 December 1

THE IMPORTANCE OF PHOTOPROCESSING IN PROTOPLANETARY DISKS

K. WILLACY[1] AND W. D. LANGER
Jet Propulsion Laboratory, California Institute of Technology, MS 169-327, Pasadena, CA 91109
Received 2000 February 23; accepted 2000 July 3

ABSTRACT

Midplane models of protoplanetary disks find that the cold temperatures in the outer parts of the disk ensure that virtually all molecules are accreted onto the grains. However, molecules in the gas are observed at these radii. One possible explanation is that the emission arises from above the midplane, possibly in a heated layer at the surface of a flared disk. Models which take into account the vertical chemical distribution of molecules and can calculate column densities are therefore required for comparison with observations. We present the results of a calculation of the time-dependent two-dimensional chemical structure of a flared protoplanetary disk which includes photoprocesses driven by both the stellar and interstellar radiation fields. Three layers are found in the disk consistent with previous work. In the upper layer photodissociation produces large abundances of atoms and ions. Below this molecules are shielded and can avoid dissociation, although sufficient radiation is present to remove molecules from the grain surfaces by photodesorption. The majority of the observable species come from this layer. Closer to the midplane of the disk, freezeout removes molecules from the gas. We find that photodesorption can account for the observed column densities if the photodesorption yield is higher than 10^{-3} molecules per photon. These results indicate that many observed molecules trace the physical and chemical conditions in the surface regions rather than the midplane although the contribution of the heated surface layer to the column densities is minimal.

Subject headings: circumstellar matter — ISM: abundances — ISM: molecules — solar system: formation — stars: formation — stars: pre–main-sequence

1. INTRODUCTION

Observations of protoplanetary disks over recent years have added greatly to our knowledge of their nature and chemical composition. These objects provide an important link in the evolution from molecular clouds to planetary systems and therefore provide a means by which we can study regions similar to the early solar system.

Detailed chemical models are required in order to help interpret these observations. The majority of previous models of protoplanetary disks have concentrated on the midplane region where the cold temperatures and high densities ensure that most molecules are accreted rapidly onto grains at $R > 100$ AU (Aikawa et al. 1997; Bauer et al. 1997; Willacy et al. 1998). Closer to the star the temperature rises, and thermal evaporation will return the molecules to the gas. Thus, different molecules reappear at different radii according to their binding energies. The radial chemical distribution is dependent on the temperature profile of the model used.

Observations, however, clearly show gaseous material at large radii. CO observations of disks have revealed that the gas extends out to several hundred AU and is moving in Keplerian motion about the central star (see Mundy, Looney, & Welch 2000 and references therein). Several other molecules have been observed by Dutrey, Guilloteau, & Guélin (1997) (HCN, HNC, CN, CS, H_2CO, HCO^+, C_2H, and N_2H^+) in addition to isotopes of CO in the outer disks ($100 < R < 900$ AU) of DM Tau and GG Tau. Both these sources are relatively old (GG Tau: $\sim 5 \times 10^5$ yr; DM Tau: $\sim 5 \times 10^6$ yr) and are therefore no longer surrounded by their parent cloud. All the molecules observed are underabundant compared with their abundances in a typical dark cloud core. These depletions range from a factor of 5 for CO to 100 for H_2CO and have been interpreted as indicating accretion onto dust grains with greater depletion for the less volatile species. Similar depletions are seen for CS toward HL Tau by Blake, van Dishoeck, & Sargent (1992) and for HCN in B5 IRS 1 (Langer, Velusamy, & Xie 1996). The midplane models do not explain these observations, and it has been suggested that the emission may arise closer to the surface of the disk (Goldsmith, Langer, & Velusamy 1999). Instead, we need models which consider the vertical structure of the disk and which can predict the column densities of observable molecules.

To date, only one previous model has considered the vertical chemical distribution in the disk. Aikawa & Herbst (1999) considered the region from the midplane to the height where the UV field is reduced to the level of the standard interstellar radiation field. They assumed the temperature to be isothermal with height. In their models the molecules are initially all gaseous, and they find appreciable column densities of several observed molecules in the gas at times of 3×10^5 yr. Freezeout causes a marked decrease (a factor of 10 in many cases) in the column densities by 9.5×10^5 yr. A comparison of the calculated fractional abundances in the outer disk with the observations of Dutrey et al. (1997) show reasonable agreement for several molecules (exceptions are CS and H_2CO).

It is thought that protostellar disks are flared allowing them to absorb more of the stellar radiation at large distances from the star than a flat disk would be able to. This results in the formation of a layer of warm gas and dust at the surface of the disk (Chiang & Goldreich 1997, hereafter CG97). The chemical effects of such a layer are considered for the first time in this paper. At large radii the temperature is not expected to be sufficiently high to cause thermal desorption, and additional desorption processes are required. Furthermore, it is thought that the warm layer will be very thin, possibly only extending for $A_V = 1$–2 mag

[1] Karen.Willacy@jpl.nasa.gov.

(CG97), and therefore not have detectable molecular column densities. An alternative desorption process that will act over larger column densities is therefore required to have molecules in the gas phase out to large radii in the disk.

Aikawa & Herbst (1999) simulated the effects of desorption by using a reduced sticking coefficient to lower the freezeout rate and starting with molecules in the gas phase. In this paper we have used a different approach by explicitly including a possible desorption process—photodesorption—and by assuming that molecules are depleted onto grains before they enter the disk.

Recent lab work by Westley et al. (1995) has found that photodesorption may be considerably more efficient than has previously been thought (see § 3.2). If this is correct, then it provides a means of removing grain mantles in the surface layers of the disk. In this paper we consider the chemical distribution in all layers of the disk from the midplane to the surface and include the effects of the UV field, both in raising the temperature of the surface layers and in the photodesorption of mantles. In the next sections we describe the physical and chemical models that we have adopted. In § 4 we present our results and compare them with the available observations. We consider also the effects of the photodesorption yield on the results. Finally, our conclusions are given in § 6.

2. THE PHYSICAL MODEL OF THE DISK

Observations clearly show that disks can extend out to several hundred AU (see Mundy et al. 2000 and references therein). Dynamical models, however, concentrate on the inner regions ($R < 300$ AU). Aikawa & Herbst (1999) extrapolated the minimum mass solar nebula model out to large radii in order to model the chemistry out to $\sim$1000 AU. We have chosen to use an extrapolation of the flared disk model of CG97. The original CG97 model describes the disk out to 270 AU. The extrapolation of the model provides a guideline to the density and temperature conditions in the outer disk and is not intended as a detailed description of the region. The derived temperatures and densities are similar to those used by Aikawa & Herbst (1999). For the outer part of the disk, we have used the expressions of CG97 for the interior temperature and disk height for $R > 209$ AU. At all radii the density at a height z above the midplane is given by

$$n(z) = n_0 \exp\left[-z^2/(2h^2)\right], \quad (1)$$

where h is the scale height of the disk. Following CG97 we set $H/h = 4$ at all radii, where H is the height of the visible photosphere above the disk midplane. The reader is referred to CG97 for further details of the model.

Here we present our results in terms of the total hydrogen number density [i.e., $n = 2n(\mathrm{H}_2) + n(\mathrm{H})$]. The midplane density, $n_0(\mathrm{H}_2)$, is taken from Figure 7 of CG97. We assume that the vertical temperature distribution of the disk is isothermal except for the thin superheated layer at the surface of the flared disk. In this region the temperature is given in Figure 4 of CG97. Models of high-density photodissociation regions (PDRs) show that the UV photons can raise the temperature of the irradiated gas to a depth of a few magnitudes of extinction. In Sternberg & Dalgarno (1995) the temperature generated in a PDR of density 10^6 cm^{-3} illuminated by a UV field of $2 \times 10^5 G_0$ (where G_0 is the standard interstellar radiation field) varies from 3000 K at $A_V = 0$ mag to 20 K at $A_V = 2.5$ mag. This radiation field is somewhat higher than would be expected in the outer regions of the disk, but similar models that we ran (unpublished) for the UV fields and densities expected in disks also show that the temperature drops sharply within an A_V of 2–3 mag. We have therefore assumed that the superheated layer extends only for less than 1 mag of visual extinction from the central star and beyond this the gas is at the midplane temperature. PDR models also show that the gas in the hot layer can be considerably warmer than the dust, although the dust and gas reach the same temperature within an A_V of about 4 mag. We have assumed that the gas and dust temperatures are always the same, consistent with the strong gas-dust coupling at the densities found in the disk.

At the surface of the disk both the radiation from the star and the interstellar radiation field must be taken into account. The stellar radiation field has been estimated to be as high as $10^4 G_0$ at 100 AU (Herbig & Goodrich 1986). We assume the standard value of the interstellar radiation field of G_0. However, the incident angles of the two fields are different, and they experience different extinctions since the path through the disk, and therefore the column density through which the photons travel, is different (see Fig. 1).

The column density measured vertically through the disk can be found by integrating equation (1). The column density from the midplane to the disk surface is given by

$$N_{\mathrm{tot}} = n_0 h \sqrt{\frac{\pi}{2}} \quad (2)$$

and the column density from height z to the edge of the disk by

$$N(z \rightarrow \infty) = n_0 h \sqrt{\frac{\pi}{2}} \left[1 - \mathrm{erf}\left(\frac{z}{\sqrt{2}h}\right)\right]. \quad (3)$$

We define the extinction experienced by the stellar UV as A_V^* and that by the interstellar radiation field as A_V^{IS}. In general, at a given point in the disk the stellar UV is subject

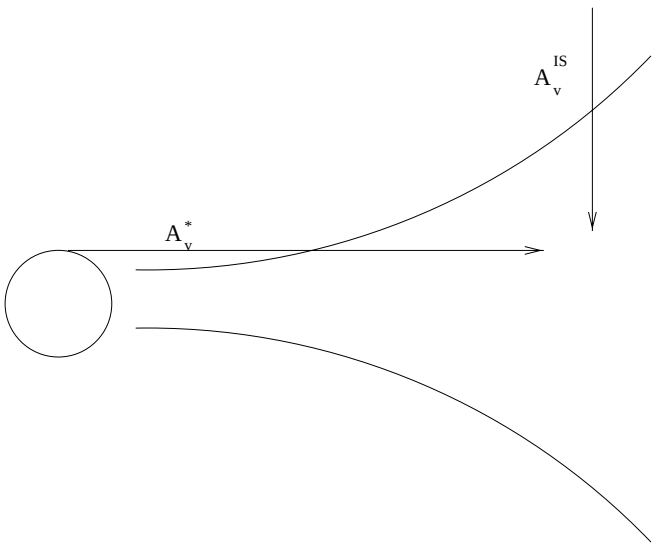

FIG. 1.—Structure of a flared irradiated disk showing the two incident UV fields (stellar and interstellar). A_V^* is the visual extinction experienced by the stellar radiation, and A_V^{IS} is the extinction experienced by the interstellar radiation field.

to a higher extinction (A_V^*) than the interstellar field (A_V^{IS}). Extinction A_V is related to the column density by $A_V = 6.1 \times 10^{-22} N_{tot}$. In order to determine the visual extinction, the column density of H_2 through which the photons pass is required. In the case of the interstellar radiation field, this is found from equation (3). For the stellar radiation field, $N(H_{tot}^*)$ is estimated by dividing the distance between the star and the radius, R, under consideration into equal slabs of width dR. The column density is then found from

$$N(H_{tot}^*) = \sum n_0 \exp(-z^2/2h^2)\, dR \quad (4)$$

for the required z where n_0 is the midplane density at each value of R. This is a rough approximation which assumes that the photons travel through the disk horizontally. In practice this is not the case. However, at the large radii which are of most importance to our model, the inclination angle of the photons will be small and the approximation is justified.

We consider six different radii and calculate the time-dependent chemical abundances for each radii vertically through the disk. Calculations are performed at regular z-intervals and the column densities estimated by integrating vertically through the disk. The parameters used in the model are given in Table 1.

3. THE CHEMICAL MODEL

3.1. *The Reaction Network*

We have used the chemical network of Willacy et al. (1998). The reaction rates are taken from the UMIST rate file (Millar, Farquhar, & Willacy 1997). We consider 172 gas and 69 solid species containing H, He, C, N, O, S, Si, Fe, and Mg, linked by 2640 reactions.

Our model considers the irradiation of the disk by UV photons from both the star and the interstellar radiation field. The physical effects of UV (i.e., increased temperature in the surface layers of the disk) are already included in the CG97 model. Chemically, the UV field will cause photodissociation, ionization, and photodesorption. Photodesorption is discussed in more detail in § 3.2. CO and H_2 self-shielding are included using the tables provided by Lee et al. (1996) for both interstellar and stellar radiation. The column densities of CO and H_2 are calculated by taking their fractional abundance at a given position and multiplying by the total column density (determined as in § 2).

Cosmic rays dominate ionization in material where the surface density is less than about 96 g cm^{-2} (Umebayashi & Nakano 1981). The surface density of the CG97 model is given by $\Sigma = R^{-3/2}\Sigma_0$, where $\Sigma_0 = 1000$ g cm^{-2}. Cosmic rays can therefore penetrate the disk for $R > 4.8$ AU, well within the smallest radius considered here, and their ionization effects have been included in our models at all radii.

Prasad & Tarafdar (1983) showed that cosmic rays can generate a secondary UV field in an otherwise shielded region. In molecular clouds these photons can cause chemical effects where the external field cannot reach. The cosmic-ray–induced photon field has been included here both for its chemical effects and for desorption (for details see Hartquist & Williams 1990). The strength of the field is considerably less than either the stellar or interstellar field, and its contribution to photodesorption is minimal. It does, however, affect the gas-phase abundances by causing photodissociation.

Two other desorption processes have been included which are more efficient than desorption by the induced UV field–cosmic-ray heating of grains and thermal desorption. Cosmic rays are responsible for keeping some molecules in the gas in the outer disk but are not the dominant process. Thermal desorption becomes increasingly important at small radii, but at 50 AU (the innermost position considered here) the temperature is only 28 K; hence, only weakly bound molecules such as CO and N_2 are evaporated. Neither process can keep a sufficient number of molecules in the gas at large radii to account for the observations.

3.2. *Photodesorption*

Desorption of ice mantles can occur by the absorption of UV photons. The photon excites the adsorbed molecule to a state which is either antibonding to the surface (i.e., has a repulsive potential) or decays to the ground state in an excited rovibrational state and some of the kinetic energy is converted into translational energy away from the surface. Early experimental work suggested that the yield per photon was very low with Greenberg (1973) assigning a value between 10^{-6} and 10^{-7} and Bourdon, Prince, & Duley (1982) a value of 10^{-10} for strongly physisorbed species. Recent experimental results have shown that this process may be more efficient than was previously thought (Westley et al. 1995). They find that in the case of water ice the desorption rate depends on the total dose of UV received by the sample and on its temperature. They measure yields of up to 3.5×10^{-3} molecules per photon for water adsorbed onto a gold electrode at 35 K. The measured yield per photon increases with the photon dose until a saturation point is reached after a total dose of $\sim 4 \times 10^{18}$ photons cm^{-2} s^{-1} at 35 K. The dose required to reach saturation depends on the temperature. We have taken the measured yields at saturation and, in the absence of data for other molecules, we have assumed that all molecules will desorb at the same rate. Similar assumptions

TABLE 1

THE PHYSICAL CONDITIONS AT EACH VALUE OF R CONSIDERED HERE

Radius (AU)	Midplane Density n_0 (cm^{-3})[a]	Interior Temperature T_i (K)	Surface Temperature T_s (K)	Maximum A_V^{IS}	N_{tot} (cm^{-2})[a]
1000.....	8.0(5)	10.8	35.3	3.33	5.46(21)
800	1.5(6)	11.9	38.7	4.67	7.65(21)
600	3.3(6)	13.5	43.6	7.21	1.18(21)
300	2.3(7)	18.0	57.9	20.5	3.36(22)
100	5.0(8)	21.0	90.8	93.5	1.53(23)
50	3.5(9)	28.1	120.7	263.0	4.32(23)

[a] Values are $A(B) = A \times 10^B$.

TABLE 2

THE FRACTIONAL ABUNDANCES OF MAJOR SPECIES RELATIVE TO THE TOTAL HYDROGEN DENSITY n_H AT THE START OF THE DISK MODEL

Species	$n(x)/n_H$	Species	$n(x)/n_H$
CO	1.8(−4)	O_2	5.2(−6)
NO	1.0(−6)	H_2O	4.8(−4)
CO_2	1.4(−7)	CH_4	1.1(−5)
HNC	8.4(−7)	H_2CO	2.0(−7)
C_2H_3	4.8(−7)	HC_3N	1.4(−7)
N_2	1.8(−5)	CH_2CO	1.0(−8)
HCN	1.0(−6)	NH_3	4.0(−6)
C_4H_2	1.9(−6)	C_3H_4	2.4(−6)
CH_3CN	4.0(−8)	CH_3OH	4.0(−6)
C_2S	2.0(−9)	H_2S	3.4(−9)
SO_2	6.0(−6)	H_2CS	1.6(−8)
SiO	1.2(−8)	SiH_4	4.2(−9)
Fe	6.0(−9)	Mg	4.0(−8)

NOTES.—These abundances are generated in a molecular cloud model including freezeout which is allowed to run for 10 Myr. All abundances refer to abundances on the grain. Values are $A(B) = A \times 10^B$.

were made for silicon compounds by Walmsley, Pineau des Forêts, & Flower (1999). In reality, small molecules will be photodesorbed more easily than large ones since they have smaller binding energies and fewer transitions by which to lose the energy imparted to them by the incident photon.

3.3. *Freezeout and Grain Surface Reactions*

The sticking efficiency of molecules onto cold grains is expected to be high (Pickles & Williams 1977). We assumed that the sticking coefficient $S_x = 1$ for all species (both molecular and atomic) other than H, H_2, and He. The sticking coefficient is expected to depend on temperature, but this has not been taken into account in the present work, except in the case of hydrogen. Ions which collide with grains stick and are neutralized in the same way as they would be if they reacted with an electron in the gas phase.

For H and H_2 we have used the temperature-dependent sticking coefficient given by Buch & Zhang (1991). They found that the sticking probability below 300 K could be described by

$$S_H(T) = [(kT/E_0) + 1]^{-2}, \quad (5)$$

where $E_0 = 102$ K for hydrogen atoms and T is the grain temperature. One consequence of this temperature dependence is that the formation rate of H_2 is reduced at higher temperatures. He is assumed not to stick.

The rates for surface reactions are not well known. They are usually estimated by assuming that hydrogen atoms and molecules can tunnel through the potential barriers between sites on the grains and thus can scan the entire grain very quickly. Heavy atoms can hop from one site to another, and molecules are immobile (see Herbst 1993). In addition, there is considerable debate about the way in which the abundances should be calculated. In order to carry out a time-dependent calculation, abundances are usually determined using a rate equation method in the same way that gaseous abundances are calculated. Tielens & Charnley (1997) showed that this is not correct and recommended a Monte Carlo approach. However, to date this has only been done for models without time dependence (Tielens & Hagen 1982) or for a time-dependent model excluding gas-grain interactions (Charnley 1998). Shalabiea, Caselli, & Herbst (1998) have suggested modifications to the rate equations to bring the results into line with Monte Carlo calculations and have compared the results from the modified equations with those from unmodified equations. They find that there are some discrepancies but that these are highly dependent on the initial form of hydrogen. If hydrogen is initially molecular, as in our models, then there are significant differences in the calculated grain mantle abundances at early times, but the results from the two models tend to converge at late times. Since our model has evolved for 10^7 yr before entering the disk phase, the inputs used for the disk should be close to the Monte Carlo results for a cloud core.

An additional uncertainty is that the grains in much of the disk are at temperatures greater than 10 K. We have used the rates calculated at 10 K which may be an underestimate for some reactions between heavy atoms and molecules since the rate is proportional to $\exp(-E_a/kT)$ and hence will rise with T. For most of the models, the temperatures are close to 10 K, so the difference in rates caused

TABLE 3

THE CALCULATED COLUMN DENSITIES FOR SEVERAL DIFFERENT RADII AT 0.5 Myr

Species	50 AU	100 AU	300 AU	600 AU	800 AU	1000 AU
CO	1.0(19)	8.6(16)	7.2(16)	7.0(16)	6.7(16)	5.3(16)
H_2CO	1.8(8)	5.7(10)	4.5(10)	2.7(11)	7.3(11)	1.4(12)
CH_3OH	1.3(10)	8.6(11)	4.4(11)	2.0(12)	3.1(12)	3.5(12)
HCO^+	1.1(13)	7.7(10)	5.1(10)	1.6(11)	1.9(11)	2.5(11)
N_2H^+	7.9(9)	1.0(13)	1.2(12)	8.2(11)	2.6(10)	2.9(10)
CN	1.5(10)	1.8(11)	4.0(11)	8.8(11)	3.1(12)	5.3(12)
HCN	1.5(10)	3.0(12)	1.4(12)	1.2(12)	2.4(12)	3.2(12)
HNC	1.3(13)	7.2(11)	2.6(11)	5.6(11)	9.8(11)	1.2(12)
C_2H	3.6(8)	3.6(10)	1.0(12)	1.6(12)	3.8(12)	5.8(12)
CS	1.5(10)	3.2(9)	9.3(10)	1.7(11)	3.9(11)	5.9(11)
SO	2.2(14)	1.4(13)	1.4(13)	1.4(13)	1.4(13)	1.6(13)
SO_2	2.9(14)	2.5(13)	2.1(13)	2.0(13)	2.0(13)	2.2(13)
H_2S	1.3(12)	3.1(12)	2.1(10)	6.0(10)	1.8(12)	7.5(11)
H_2	2.1(21)	7.5(22)	1.6(22)	5.6(21)	3.5(21)	2.2(21)

NOTES.—The photodesorption yield is taken to be Y_0 (i.e., the value given in Westley et al. 1995 for H_2O). Values are $A(B) = A \times 10^B$.

TABLE 4

THE CALCULATED COLUMN DENSITIES FOR SEVERAL DIFFERENT RADII AT 1 Myr

Species	50 AU	100 AU	300 AU	600 AU	800 AU	1000 AU
C^+	5.4(16)	5.7(16)	8.4(16)	6.8(16)	2.9(16)	2.0(15)
C	1.1(14)	1.2(14)	3.4(15)	4.7(15)	4.0(15)	6.5(14)
CO	1.0(19)	8.6(16)	7.2(16)	7.0(16)	6.7(16)	5.4(16)
CO_2	2.8(12)	6.2(11)	1.8(12)	2.3(12)	2.4(12)	2.8(12)
H_2CO	1.2(8)	1.2(10)	3.1(10)	2.0(11)	4.8(11)	9.1(11)
CH_3OH	1.1(10)	1.8(11)	3.6(11)	1.6(12)	2.3(12)	2.3(12)
HCO^+	1.1(13)	7.8(10)	5.2(10)	1.6(11)	1.9(11)	2.6(11)
N_2	2.1(18)	2.3(17)	7.1(16)	1.1(16)	2.0(15)	1.5(15)
NH	3.6(13)	5.7(13)	8.8(12)	4.2(12)	3.1(12)	5.8(12)
NH_3	1.7(11)	1.6(13)	1.2(13)	1.7(13)	6.8(12)	1.0(13)
N_2H^+	1.3(10)	9.5(12)	8.7(11)	6.9(11)	2.6(10)	2.8(10)
NO	6.9(13)	8.3(13)	7.8(13)	8.5(13)	8.0(13)	9.8(13)
NS	3.6(9)	6.5(12)	2.4(10)	3.1(10)	1.2(13)	8.0(12)
CN	1.1(10)	1.9(11)	4.1(11)	7.7(11)	2.6(12)	4.3(12)
HCN	1.6(10)	3.5(12)	1.5(12)	1.2(12)	2.3(12)	3.0(12)
HNC	1.0(13)	6.6(11)	2.1(11)	4.9(11)	8.2(11)	9.6(11)
HC_3N	4.8(8)	7.4(9)	1.1(10)	2.3(10)	3.2(10)	2.8(10)
CH_3CN	1.3(8)	2.3(9)	4.1(9)	1.5(10)	2.1(10)	2.0(10)
CH	4.4(12)	1.5(10)	6.0(11)	1.1(12)	2.2(12)	2.4(12)
CH_4	7.3(16)	4.2(15)	6.8(12)	7.5(12)	1.3(13)	1.6(13)
C_2H	3.0(8)	1.5(10)	7.3(11)	1.2(12)	2.8(12)	4.1(12)
C_3H	4.5(8)	7.6(11)	2.2(11)	5.4(11)	1.5(12)	2.1(12)
C_4H	9.8(7)	8.9(8)	4.8(10)	2.7(11)	4.6(11)	4.5(11)
C_2H_2	5.3(11)	6.5(9)	1.8(11)	2.9(11)	5.3(11)	6.0(11)
C_3H_2	4.5(7)	7.4(11)	2.0(11)	4.7(11)	1.2(12)	1.7(12)
C_3H_4	1.2(11)	4.5(12)	4.1(11)	1.1(12)	1.8(12)	1.8(12)
O	4.3(17)	2.5(17)	3.0(17)	2.6(17)	1.6(17)	7.5(16)
OH	3.2(13)	8.5(13)	1.3(14)	2.2(14)	3.6(14)	5.0(14)
H_2O	2.9(14)	2.8(14)	2.3(14)	3.4(14)	5.3(14)	6.8(14)
CS	1.5(10)	2.6(9)	8.4(10)	1.4(11)	3.1(11)	4.6(11)
C_2S	7.4(6)	2.7(9)	9.0(9)	1.6(10)	1.0(11)	2.2(11)
SO	2.2(14)	1.4(13)	1.4(13)	1.4(13)	1.4(13)	1.6(13)
SO_2	2.9(14)	2.5(13)	2.1(13)	2.0(13)	2.0(13)	2.2(13)
H_2S	1.3(12)	3.1(12)	2.1(10)	6.1(10)	1.8(12)	7.5(11)
HCS	2.5(6)	1.2(7)	7.8(8)	2.0(9)	5.2(9)	7.5(9)
SiH	1.6(5)	2.6(5)	8.6(7)	1.3(8)	1.2(8)	1.5(8)
SiH_4	1.8(13)	6.8(12)	1.9(12)	2.4(12)	2.8(12)	2.2(12)
SiO	6.5(8)	1.5(10)	2.2(10)	3.8(10)	4.7(10)	7.1(10)
SiO_2	1.1(12)	1.8(11)	2.1(11)	1.8(11)	1.6(11)	1.3(11)
SiC	1.2(5)	4.4(7)	1.8(8)	2.5(8)	4.2(8)	5.5(8)
H_2	2.1(23)	7.5(22)	1.6(22)	5.5(21)	3.5(21)	2.2(21)

NOTES.—The photodesorption yield is taken to be Y_0 (i.e., the value given in Westley et al. 1995 for H_2O). Values are $A(B) = A \times 10^B$.

by the temperature will be small. The rates and the molecular binding energies are taken from Hasegawa, Herbst, & Leung (1992) and Hasegawa & Herbst (1993) with additional binding energies from the experimental results of Sandford & Allamandola (1993).

3.4. *Initial Abundances*

The input abundances are generated by adopting a molecular cloud model with a density of 2×10^4 cm^{-3}, $T = 10$ K, and $A_V = 10$ mag, physical conditions which are characteristic of preprotostellar cores. The model is allowed to run for 10 Myr and includes freezeout but not desorption. Hence, all molecules are accreted onto the grains. Observations, for example, Mezger et al. (1992) and Willacy, Langer, & Velusamy (1998), have shown that molecules in dense molecular cloud cores are strongly depleted. As collapse continues the density will rise and the freezeout rate will increase. It is therefore logical to assume that most, if not all, species in the infalling material could be frozen onto the grains when they enter the disk.

The effects on the dust of passing through the accretion shock at the disk surface have been modeled by several authors, e.g., Chick & Cassen (1997) and Lunine et al. (1991). Chick & Cassen (1997) found that vaporization of ices could occur between 2 and 30 AU, depending on the luminosity of the central star and the characteristics of the collapsing cloud. This distance range is within the innermost radius considered here. Lunine et al. (1991) showed that once in the nebula the vaporized gas will cool rapidly and recondense on the grains, possibly trapping other volatiles in the ice. The amount of evaporation and recondensation depends on the distance from the star and is most efficient for $R < 50$ AU. At the larger radii of interest in this paper, little evaporation is expected. Both these results support our assumption that initially all molecules are part of the grain mantles.

TABLE 5

THE CALCULATED COLUMN DENSITIES FOR SEVERAL DIFFERENT RADII AT 5 Myr

Species	50 AU	100 AU	300 AU	600 AU	800 AU	1000 AU
CO	2.3(17)	8.6(16)	7.2(16)	7.0(16)	6.7(16)	5.4(16)
H_2CO	9.0(7)	3.1(8)	2.2(10)	9.0(10)	2.3(11)	4.7(11)
CH_3OH.....	8.6(9)	2.0(9)	2.9(11)	6.7(11)	8.8(11)	5.6(11)
HCO^+	1.8(11)	1.0(11)	5.7(10)	1.6(11)	2.0(11)	2.6(11)
N_2H^+	3.3(11)	7.4(11)	2.6(11)	2.0(11)	2.4(10)	2.7(10)
CN	1.4(9)	2.2(11)	3.3(11)	9.0(11)	2.2(12)	3.4(12)
HCN	1.7(10)	4.2(12)	1.2(12)	1.7(12)	2.5(12)	3.0(12)
HNC	2.9(12)	7.3(11)	1.7(11)	4.6(11)	6.6(11)	7.4(11)
C_2H	2.7(7)	1.2(11)	7.4(10)	5.6(11)	8.6(11)	1.1(12)
CS	1.5(10)	2.5(9)	8.0(10)	1.0(11)	2.6(11)	3.6(11)
SO.....	2.2(14)	1.4(13)	1.4(13)	1.4(13)	1.4(13)	1.6(13)
SO_2	2.9(14)	2.5(13)	2.1(13)	2.0(13)	2.0(13)	2.2(13)
H_2S	1.3(12)	3.1(12)	2.1(10)	6.3(10)	1.8(12)	7.6(11)
H_2	2.1(23)	7.5(22)	1.6(22)	5.3(21)	3.3(21)	2.2(21)

NOTES.—The photodesorption yield is taken to be Y_0 (i.e., the value given in Westley et al. 1995 for H_2O). Values are $A(B) = A \times 10^B$.

Usually, molecular cloud models begin with all elements in their atomic or ionic forms and with a relatively large H/H_2 ratio. This results in the efficient formation on grains of hydrogenated species such as NH_3 and CH_4 at early times, leading to much higher abundances of these species than are observed in the solid state in clouds. We have attempted to address this problem by assuming that at the start of the molecular cloud model the gas has already begun to evolve. We assume that initially the carbon is divided up among $CO:C:C^+$ in the ratio 0.5:0.25:0.25. Similarly, nitrogen is assumed to be partially in N_2 with only 20% being atomic. Oxygen is atomic except for that fraction which is in CO (the H_2O abundance is expected to be low under these conditions). In addition, we have taken H/H_2 to be $1/n_{\rm H}$ (the ratio which is seen at late times in chemical models). These changes ensure that grain hydrogenation is less efficient, resulting in a factor of 10 reduction in the abundances of solid CH_4 and NH_3 compared to the atomic input model. The methanol abundance is reduced by a similar amount. The abundance of other molecules on the grain (including water which is formed efficiently by hydrogenation of oxygen atoms on the grains) is not affected. We find that the gas-phase abundances at 1 Myr do not depend critically on the initial conditions.

The choice of disk input abundances is important. Willacy et al. (1998) found that the abundances of some molecules are unaltered by processing in the disk and therefore reflect their input values.

Molecular cloud models tend to assume that the sulphur is severely depleted, by 2–3 orders of magnitude with respect to the solar abundance (e.g., Millar & Herbst 1990; Lee et al. 1998; Williams 1998) with the missing sulphur generally assumed to be accreted onto icy grain mantles. For example, the low metal abundances used by Graedel, Langer, & Frerking (1982) and Leung, Herbst, & Huebner (1984) have a fractional abundance relative to $n_{\rm H}$ of $x(S) \sim 1.6 \times 10^{-7}$ compared to its cosmic abundance of 1.6×10^{-5}. We found that using such high depletions in our molecular cloud model resulted in very low abundances of sulphur-bearing molecules in the disk models and, therefore, in column densities far lower than observed. Comet observations, on the other hand, show a high abundance of sulphur molecules with an abundance relative to water ice of 0.028 (see Irvine et al. 2000), i.e., $x(S) = 5.6 \times 10^{-6}$, if the

TABLE 6

THE CALCULATED FRACTIONAL ABUNDANCES RELATIVE TO H_2 FOR SEVERAL DIFFERENT RADII AT 0.5 Myr

Species	50 AU	100 AU	300 AU	600 AU	800 AU	1000 AU
CO*	4.8(−5)*	1.1(−6)	4.5(−6)*	1.3(−5)*	1.9(−5)*	2.4(−5)*
H_2CO*	8.6(−16)	7.6(−13)	2.8(−12)	4.9(−11)	2.1(−10)*	6.4(−10)*
CH_3OH.....	6.2(−14)	1.1(−11)	2.7(−11)	3.6(−10)	9.0(−10)	1.6(−9)
HCO^+*.....	5.2(−11)	1.0(−12)	3.1(−12)	2.8(−11)	5.4(−11)	1.1(−10)
N_2H^+*.....	3.8(−14)*	1.4(−10)*	7.7(−11)*	1.5(−10)*	7.5(−12)*	1.3(−11)*
CN*	7.1(−14)	2.3(−12)	2.5(−11)	1.6(−10)	9.0(−10)*	2.4(−9)*
HCN*.....	7.1(−14)	4.0(−11)	8.5(−11)	2.1(−10)*	6.8(−10)*	1.4(−9)*
HNC*.....	6.2(−11)	9.6(−12)	1.6(−11)	1.0(−10)*	2.8(−10)*	5.5(−10)*
C_2H*.....	1.7(−14)	4.9(−13)	6.5(−11)	2.8(−10)	1.1(−9)	2.6(−9)*
CS*.....	7.1(−14)	4.3(−14)	5.8(−12)	3.1(−11)	1.1(−10)	2.7(−10)
SO.....	1.0(−9)	1.9(−10)	9.0(−10)	2.5(−9)	4.1(−9)	7.0(−9)
SO_2	1.4(−9)	3.4(−10)	1.3(−9)	3.7(−9)	5.7(−9)	1.0(−8)
H_2S	6.2(−12)	4.1(−11)	1.3(−12)	1.1(−11)	5.1(−10)	3.4(−10)

NOTES.—The photodesorption yield is taken to be Y_0 (i.e., the value given in Westley et al. 1995 for H_2O). Figures with asterisks agree with the observed abundances to within a factor of 5. Species shown with asterisks are those observed by Dutrey et al. 1997. Values are $A(B) = A \times 10^B$.

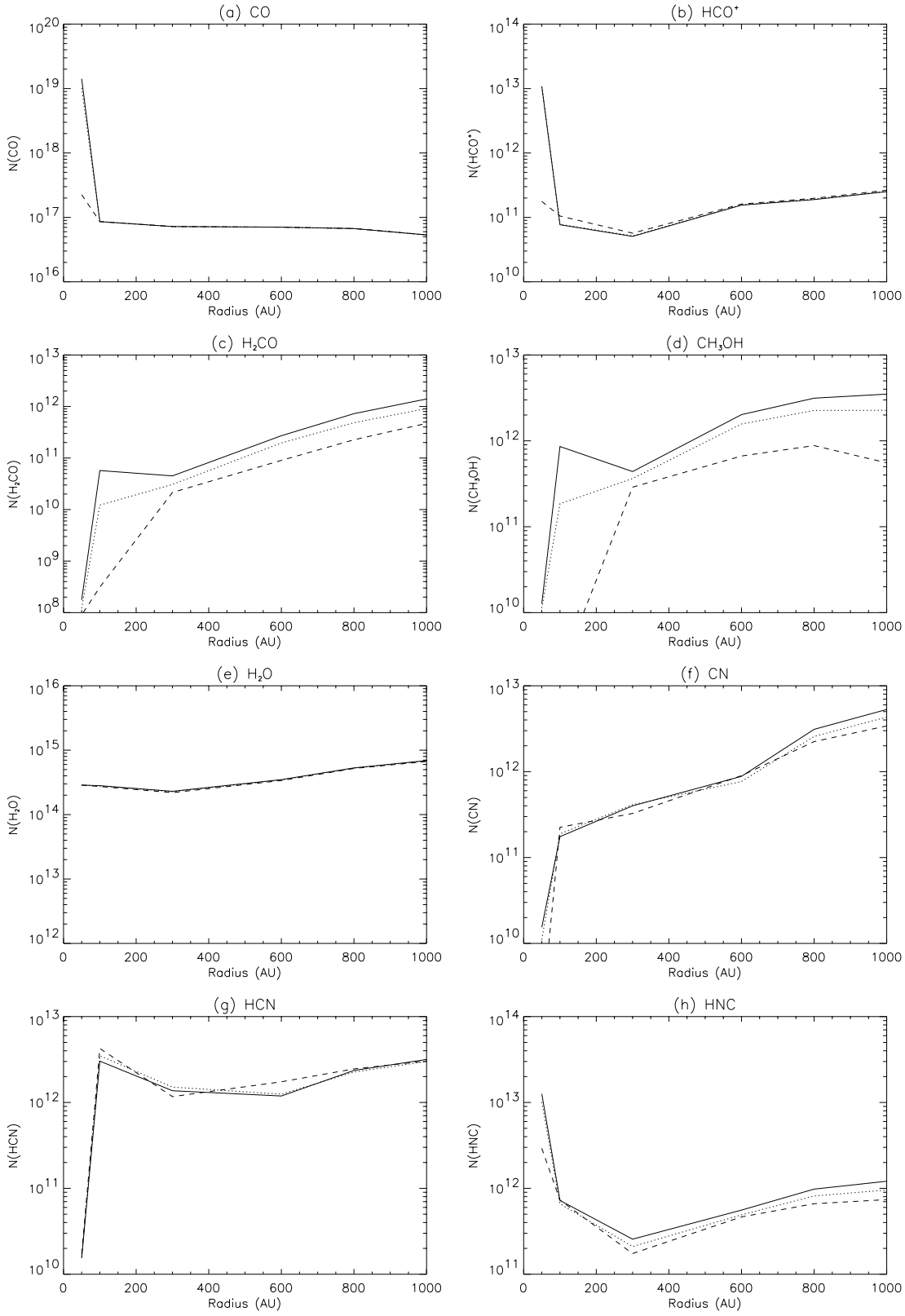

FIG. 2.—Radial distribution of calculated column density for selected species. The results at three times are shown: 0.5 Myr (*solid lines*), 1 Myr (*dotted lines*), and 5 Myr (*dashed lines*).

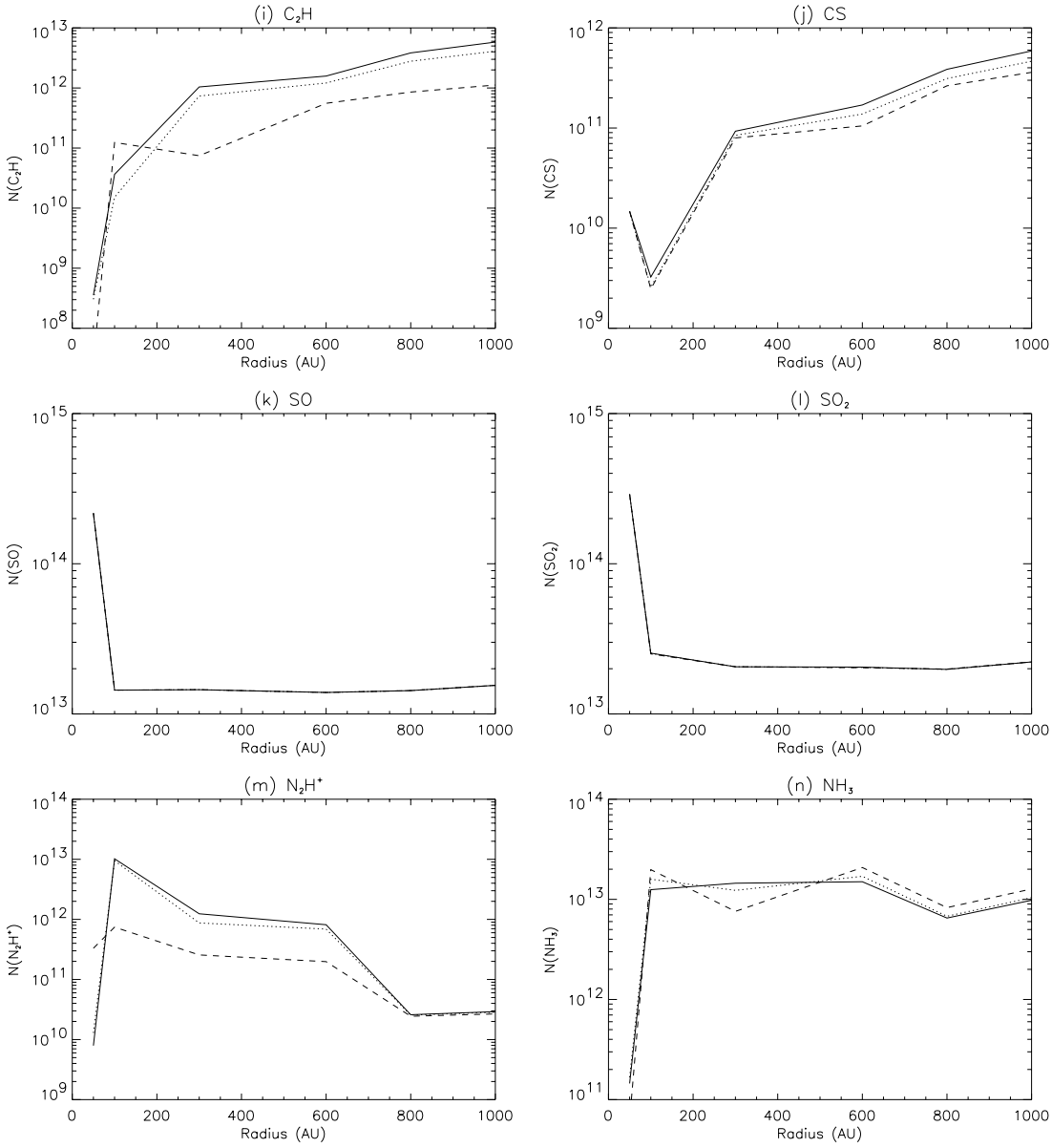

FIG. 2.—*Continued*

fractional abundance of water ice is $\sim 2 \times 10^{-4}$. We therefore used $x(S) = 6 \times 10^{-6}$ in our molecular cloud model in order to ensure a high abundance of sulphur in the disk. Initially, we started with $x(S_{gas}) = 1.6 \times 10^{-7}$, as in low–metal abundance models, and the remainder of the sulphur on the grains in atomic form.

The details of the formation process of methanol on grains are still uncertain. Our molecular cloud model results in $x(CH_3OH) \sim 10^{-8}$. This is considerably lower than the methanol abundance observed in comets ($\sim 10^{-6}$ from observations of Hale-Bopp). We have therefore assumed a fractional abundance of solid CH_3OH of 2×10^{-6} as an input to the disk model. The complete set of disk input abundances are shown in Table 2.

4. RESULTS

We have calculated both the column density and an average fractional abundance $[N(x)/N(H_2)]$ along a line perpendicular to the midplane of the disk at each radii. The results are shown in Tables 3, 4, and 5 and Figure 2 for the column densities and Tables 6, 7, and 8 and Figure 3 for the fractional abundances. We present the results for three times: 0.5 Myr, 1 Myr, and 5 Myr. For the tables of results at 0.5 and 5 Myr, we present data only for those molecules which have been observed. For 1 Myr we give a more complete list of column densities and abundances since this is the model corresponding to the estimated age of the observed systems. Abundances of other species at all times are available on request from the authors.

We find that the disk can be divided into three separate chemical layers:

The ionized layer.—At the upper surface of the disk, where the UV field is unattenuated, the grains are completely clear of mantles and the gas is ionized or atomic.

The gaseous molecular layer.—Moving farther down, the UV begins to be absorbed, allowing molecules to form. Photodesorption is still efficient, and most of the material is in the gas.

The ice layer.—Finally, when $A_V^{IS} > 4$ mag the UV field

TABLE 7

THE CALCULATED FRACTIONAL ABUNDANCES RELATIVE TO H_2 FOR SEVERAL DIFFERENT RADII AT 1 Myr

Species	50 AU	100 AU	300 AU	600 AU	800 AU	1000 AU
C^+	2.6(−7)	7.6(−7)	5.2(−6)	1.3(−5)	8.3(−6)	8.9(−7)
C	5.2(−10)	1.6(−9)	2.1(−7)	8.6(−7)	1.1(−6)	3.0(−7)
CO*	4.8(−5)*	1.1(−6)	4.5(−6)*	1.3(−5)*	1.9(−5)*	2.4(−5)*
CO_2	1.3(−11)	8.3(−12)	1.1(−10)	4.2(−10)	6.8(−10)	1.3(−9)
H_2CO*	5.7(−16)	1.6(−13)	1.9(−12)	3.6(−11)	1.4(−10)*	4.2(−10)*
CH_3OH	5.2(−14)	2.5(−12)	2.3(−11)	2.9(−10)	6.6(−10)	1.0(−9)
HCO^+*	5.2(−11)	1.0(−12)	3.2(−12)	2.9(−11)	5.6(−11)	1.2(−10)
N_2	1.0(−5)	3.1(−6)	4.4(−6)	2.0(−6)	5.7(−7)	6.7(−7)
NH	1.7(−10)	7.6(−10)	5.5(−10)	7.7(−10)	9.0(−10)	2.7(−9)
NH_3	8.1(−13)	2.1(−10)	7.7(−10)	3.1(−9)	2.0(−9)	4.7(−9)
N_2H^+*	6.2(−14)*	1.3(−10)*	5.4(−11)*	1.3(−10)*	7.4(−12)*	1.3(−11)*
NO	3.3(−10)	1.1(−9)	4.8(−9)	1.6(−8)	2.3(−8)	4.5(−8)
NS	1.7(−14)	8.6(−11)	1.5(−12)	5.7(−12)	3.5(−9)	3.6(−9)
CN*	5.2(−14)	2.5(−12)	2.6(−11)	1.4(−10)	7.4(−10)*	2.0(−9)*
HCN*	7.6(−14)	4.7(−11)	9.4(−11)*	2.3(−10)*	6.6(−10)*	1.4(−9)*
HNC*	4.8(−11)	8.8(−12)	1.3(−11)	9.0(−11)*	2.4(−10)*	4.3(−10)*
HC_3N	2.3(−15)	9.9(−14)	6.9(−13)	4.3(−12)	9.2(−12)	1.3(−11)
CH_3CN	6.2(−16)	3.1(−14)	2.6(−13)	2.7(−12)	6.1(−12)	9.0(−12)
CH	2.1(−11)	2.0(−13)	3.7(−11)	2.1(−10)	6.3(−10)	1.1(−9)
CH_4	3.5(−7)	5.6(−8)	4.3(−10)	1.4(−9)	3.8(−9)	7.5(−9)
C_2H*	1.4(−15)	2.0(−13)	4.6(−11)	2.2(−10)	8.1(−10)	1.9(−9)
C_3H	2.1(−15)	1.0(−11)	1.4(−11)	9.8(−11)	4.2(−10)	9.7(−10)
C_4H	4.7(−16)	1.2(−14)	3.0(−12)	5.0(−11)	1.3(−10)	2.0(−10)
C_2H_2	2.5(−12)	8.6(−14)	1.1(−11)	5.2(−11)	1.5(−10)	2.7(−10)
C_3H_2	2.1(−16)	9.9(−12)	1.3(−11)	8.6(−11)	3.4(−10)	7.5(−10)
C_3H_4	5.7(−13)	6.0(−11)	2.6(−11)	2.0(−10)	5.1(−10)	8.0(−10)
O	2.0(−6)	3.4(−6)	1.9(−5)	4.8(−5)	4.8(−5)	3.4(−5)
OH	1.5(−10)	1.1(−9)	8.4(−9)	4.0(−8)	1.0(−7)	2.3(−7)
H_2O	1.4(−9)	3.7(−9)	1.4(−8)	6.3(−8)	1.5(−7)	3.1(−7)
CS*	7.1(−14)	3.4(−14)	5.3(−12)	2.5(−11)	9.0(−11)*	2.1(−10)*
C_2S	3.5(−17)	3.6(−14)	5.6(−13)	3.0(−12)	2.9(−11)	1.0(−10)
SO	1.0(−9)	1.9(−10)	9.1(−10)	2.5(−9)	4.1(−9)	7.0(−9)
SO_2	1.4(−9)	3.4(−10)	1.3(−9)	3.7(−9)	5.7(−9)	1.0(−8)
H_2S	6.2(−12)	4.1(−11)	1.3(−12)	1.1(−11)	5.2(−10)	3.4(−10)
HCS	1.2(−17)	1.5(−16)	4.9(−14)	3.7(−13)	1.5(−12)	3.4(−12)
SiH	7.6(−19)	3.5(−18)	5.4(−15)	2.4(−14)	3.4(−14)	6.7(−14)
SiH_4	8.6(−11)	9.1(−11)	1.2(−10)	4.4(−10)	8.0(−10)	1.0(−9)
SiO	3.1(−15)	2.0(−13)	1.4(−12)	6.9(−12)	1.4(−11)	3.2(−11)
SiO_2	5.2(−12)	2.3(−12)	1.3(−11)	3.3(−11)	4.6(−11)	6.1(−11)
SiC	5.7(−19)	5.9(−16)	1.1(−14)	4.6(−14)	1.2(−13)	2.5(−13)

NOTES.—The photodesorption yield is taken to be Y_0 (i.e., the value given in Westley et al. 1995 for H_2O). Figures with asterisks agree with the observed abundances to within a factor of 5. Species shown with asterisks are those observed by Dutrey et al. 1997. Values are $A(B) = A \times 10^B$.

intensity is too low for desorption to occur rapidly and molecules are completely frozen out.

The warm dust layer described by CG97 exists completely in the ionized layer and therefore does not contribute to the molecular column density. In the molecular layer the temperatures are at their midplane values and thermal desorption is not important over much of the disk.

The stellar UV field is mainly responsible for the warm dust layer and the ionized layer. The molecular layer forms at a point where the gas is shielded from the stellar UV, and photodesorption is mainly due to the interstellar radiation field.

Molecules show different behavior with radius. Several molecules, e.g., CO_2, H_2CO, NH_3, and CN, show a reduction in the fractional abundance with decreasing R as would be expected (the increase in density as R decreases leads to an increase in the freezeout rate, and since the temperature is still low even at 50 AU only the most volatile of species are desorbed). At 100 AU thermal desorption is not important for any species, and the difference in temperature between 100 and 50 AU can be seen in the abundance of CO, N_2, and CH_4, which are considerably higher at 50 AU. HNC is also desorbed at 50 AU, whereas HCN with a slightly higher binding energy is not.

The abundances of many species change little between 5×10^5 and 5×10^6 yr. Exceptions are CH_3OH, H_2CO, and N_2H^+. The decreases in abundance shown by these molecules are due to them being processed into other species, e.g., CH_3OH is photodissociated into either CH_3 and OH or H_2CO. Neither of these molecules are recycled back into methanol, leading to a gradual reduction in its abundance.

TABLE 8

THE CALCULATED FRACTIONAL ABUNDANCES RELATIVE TO H_2 FOR SEVERAL DIFFERENT RADII AT 5 Myr

Species	50 AU	100 AU	300 AU	600 AU	800 AU	1000 AU
CO*	1.1(−6)	1.1(−6)	4.5(−6)*	1.3(−5)*	2.0(−5)*	2.4(−5)*
H_2CO*	4.3(−16)	4.2(−15)	1.3(−12)	1.7(−11)	6.8(−11)	2.2(−10)*
CH_3OH.....	4.1(−14)	2.6(−14)	1.8(−11)	1.3(−10)	2.7(−10)	2.5(−10)
HCO^+*	8.6(−13)	1.4(−12)	3.6(−12)	3.0(−11)	6.0(−11)	1.2(−10)
N_2H^+	1.6(−12)	9.9(−12)	1.6(−11)	3.7(−11)	7.4(−12)	1.2(−11)
CN*	6.7(−15)	3.0(−12)	2.0(−11)	1.7(−10)	6.8(−10)*	1.6(−9)*
HCN*.....	8.1(−14)	5.7(−11)	7.3(−11)	3.3(−10)*	7.4(−10)*	1.4(−9)*
HNC*.....	1.4(−11)	9.7(−12)	1.1(−11)	8.8(−11)*	2.0(−10)*	3.4(−10)*
C_2H*.....	1.3(−16)	1.7(−12)	4.7(−12)	1.1(−10)	2.6(−10)	5.1(−10)
CS*.....	7.1(−14)	3.3(−14)	5.0(−12)	2.0(−11)	8.0(−11)*	1.6(−10)*
SO.....	1.0(−9)	1.9(−10)	9.1(−10)	2.6(−9)	4.3(−9)	7.1(−9)
SO_2	1.4(−9)	3.3(−10)	1.3(−9)	3.8(−9)	6.0(−9)	1.0(−8)
H_2S	6.2(−12)	4.1(−11)	1.3(−12)	1.2(−11)	5.5(−10)	3.5(−10)

NOTES.—The photodesorption yield is taken to be Y_0 (i.e., the value given in Westley et al. 1995 for H_2O). Figures with asterisks agree with the observed abundances to within a factor of 5. Species shown with asterisks are those observed by Dutrey et al. 1997. Values are $A(B) = A \times 10^B$.

4.1. *The Abundance Distribution with Height, z*

Within the molecular layer the molecules themselves show stratification. Figures 4 and 5 show the vertical distribution of several species at 800 and 100 AU, respectively. We consider the processes acting at 800 AU in order to understand the chemistry of the disk.

At 800 AU the molecules exist in the gas from $z \sim 100$ to 420 AU, with the majority of the molecules being found between $z \sim 150$ and 300 AU. CO forms higher up in the disk once self-shielding is effective. Its abundance peaks between $z = 340$ and 380 AU and is determined by the balance between freezeout and photodesorption. Inside 300 AU the abundances of atomic ions such as C^+ and S^+ fall due to the reduction in the UV ionization rate. This results in a decrease in the electron abundance and an increase in the H_3^+ abundance. H_3^+ is involved in the production of molecular ions, e.g., HCO^+ and N_2H^+, and these ions are most abundant in this region (Figs. 4*b* and 4*m*).

Near the surface of the disk gaseous water is more likely to be photodissociated than to refreeze, even within the region where CO can self-shield. This results in the production of oxygen atoms, most of which freezeout and are hydrogenated to form more water ice. Some will also react to form O_2, SO_2, and NO. At $z = 300$ AU this cycle results in a decrease in the water ice abundance with time, although little time dependence is seen in the gas-phase abundance. As z decreases, direct freezeout of water becomes more important and less oxygen is lost from H_2O.

The observation of CN in disks indicates that photodissociation is important since CN forms from the photodissociation of HCN. HCN is also removed from the gas by refreezing and by reaction with H_3^+ to form $HCNH^+$. Figure 6 shows the reaction scheme linking HCN, CN, and HNC at two values of z. In both positions HNC is gradually removed forming first CN and then when this freezes out it is processed into HCN. At lower heights the electron

TABLE 9

COLUMN DENSITIES AND FRACTIONAL ABUNDANCES (RELATIVE TO H_2) CALCULATED AT 0.5 Myr AT 800 AU FOR DIFFERENT VALUES OF THE PHOTODESORPTION YIELD, Y

	COLUMN DENSITY				$N(x)/N(H_2)$			
SPECIES	Y_0	$Y_0/3$	$Y_0/10$	$Y_0/50$	Y_0	$Y_0/3$	$Y_0/10$	$Y_0/50$
CO*	6.7(16)	4.4(16)	1.7(16)	2.5(15)	1.9(−5)*	1.3(−5)*	4.9(−6)*	7.1(−7)
H_2CO*	7.3(11)	3.9(11)	1.7(11)	4.3(10)	2.1(−10)*	1.1(−10)*	4.8(−11)	1.2(−11)
CH_3OH.....	3.1(12)	1.6(12)	6.5(11)	1.8(11)	9.0(−10)	4.5(−10)	1.9(−10)	5.1(−11)
HCO^+*	1.9(11)	9.9(10)	4.9(10)	1.6(10)	5.4(−11)	2.9(−11)	1.4(−11)	4.6(−12)
N_2H^+*	2.6(10)	1.4(10)	6.6(9)	1.4(9)	7.5(−12)	4.2(−12)	1.9(−12)	4.2(−13)
CN*	3.1(12)	2.1(12)	1.0(12)	1.7(12)	9.0(−10)*	6.1(−10)*	2.9(−10)	4.9(−10)
HCN*.....	2.4(12)	9.0(11)	2.5(11)	1.5(11)	6.8(−10)*	2.6(−10)*	7.1(−11)	4.3(−11)
HNC*.....	9.8(11)	5.0(11)	1.9(11)	1.3(11)	2.8(−10)*	1.4(−10)*	5.6(−11)*	3.8(−11)
C_2H*.....	3.8(12)	2.2(12)	1.0(12)	4.7(11)	1.1(−9)	6.4(−10)	3.0(−10)	1.4(−10)
CS*.....	3.9(11)	1.8(11)	1.2(11)	8.7(10)	1.1(−10)*	5.3(−11)	3.6(−11)	2.5(−11)
SO.....	1.4(13)	4.5(12)	1.1(12)	1.7(11)	4.1(−9)	1.3(−9)	3.2(−10)	5.0(−11)
SO_2	2.0(13)	7.0(12)	1.8(12)	2.7(11)	5.7(−9)	2.0(−9)	5.3(−10)	7.8(−11)
H_2S	1.8(12)	1.4(12)	3.2(11)	3.1(11)	5.1(−10)	4.1(−10)	9.2(−11)	9.0(−11)
H_2	3.5(21)	3.5(21)	3.5(21)	3.4(21)	1.0	1.0	1.0	1.0

NOTES.—Y_0 is the value of Y taken from Westley et al. 1995. Species observed by Dutrey et al. 1997 are shown with asterisks, and those calculated fractional abundances which are within a factor of 5 of the observed values (or which are consistent with the upper limit in the case of N_2H^+) are also indicated with asterisks. The observed values are given in Table 12. Values are $A(B) = A \times 10^B$.

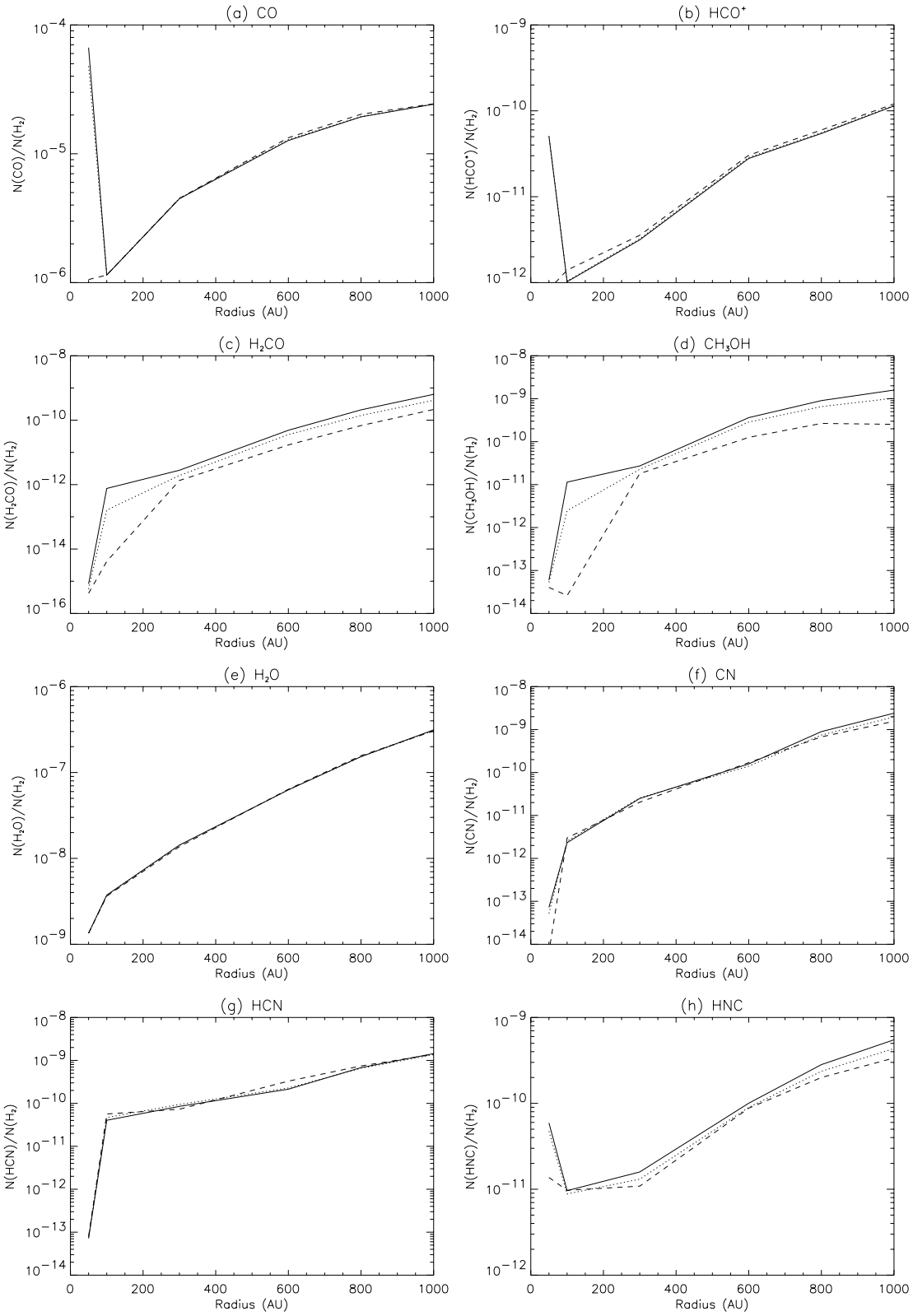

FIG. 3.—Radial distribution of $N(x)/N(\mathrm{H}_2)$. The results at three times are shown: 0.5 Myr (*solid lines*), 1 Myr (*dotted lines*), and 5 Myr (*dashed lines*).

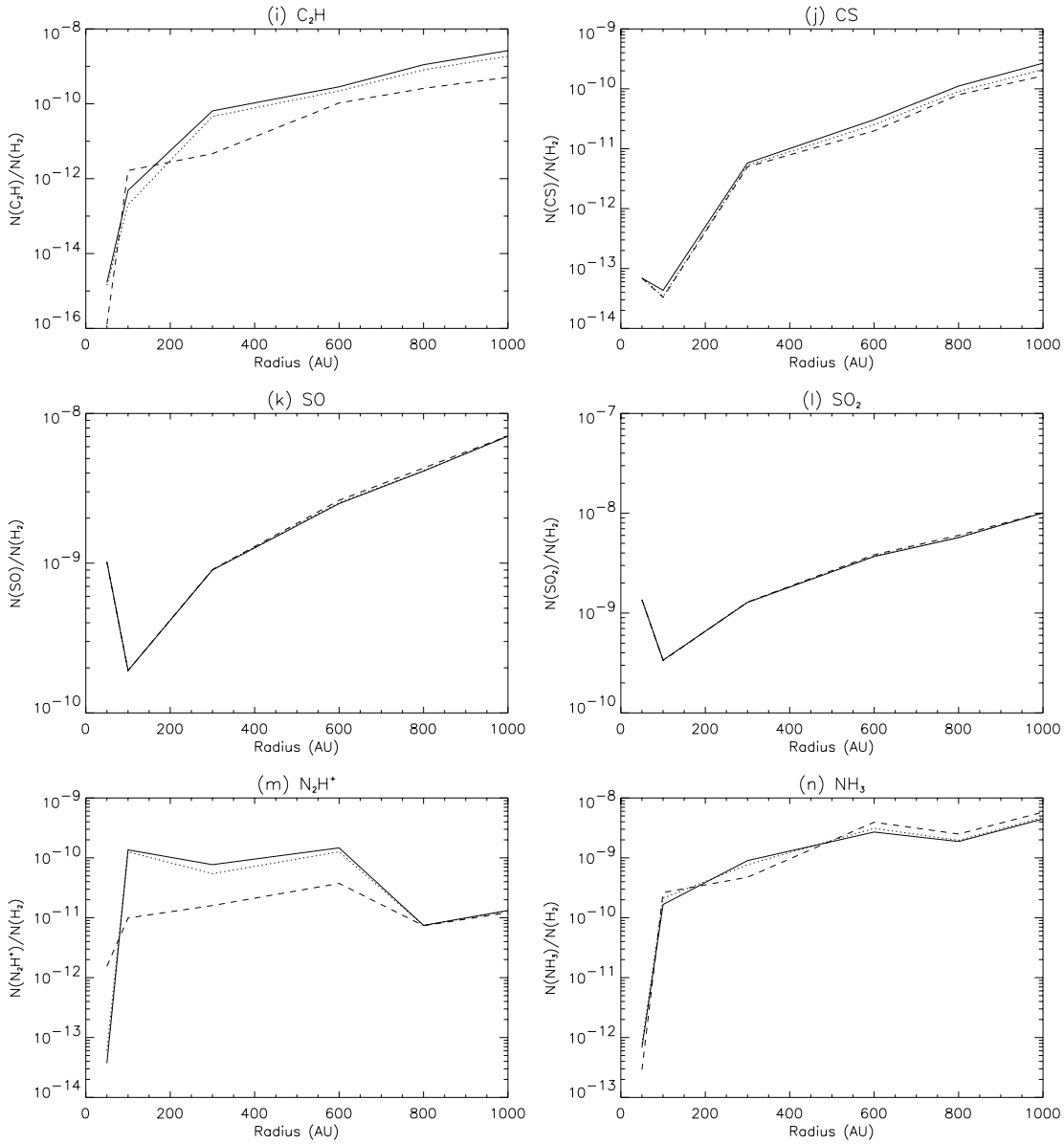

FIG. 3.—*Continued*

recombination of $HCNH^+$ becomes more important in the formation of CN and, to a lesser extent, HNC and HCN.

In the gas, the HNC/HCN ratio increases with decreasing z. Below about 100 AU most of the HCN and HNC are on the dust grains, and the solid HNC/HCN ratio is roughly constant at ~ 0.85. Above 100 AU the grain ratio reflects the gas ratio. Below 100 AU the gas ratio continues to rise but the abundance of molecules in the gas is very low. The low ratio at large values of z arises from the photodissociation of HNC into CN and its subsequent processing into HCN on the grains.

C_2H is another molecule formed by photodissociation. Its peak abundance is at $z = 240$ AU ($A_V^{IS} = 1.8$, $A_V^* = 5.5$). At this point it forms from the destruction of C_2H_2 and is itself destroyed either by photodissociation or by freezeout. At smaller z dissociation of other hydrocarbons becomes more important, e.g., C_4H_2, C_4H. However, the process is not efficient enough to produce the column densities of C_2H observed.

Photodesorption of H_2CO only contributes directly to the gas-phase abundance at early model times. At the times we consider here it is produced in the gas mainly by the reaction of O and CH_3 with a smaller contribution from the photodissociation of methanol. The latter process gradually begins to dominate the formation of H_2CO as z decreases. H_2CO is removed either by freezeout or, at high z, by photodissociation. In the mantle, H_2CO is constantly cycled to HCO and back by reaction with H atoms and OH radicals.

4.2. *The Effect of the Efficiency of the Photodesorption Process*

Tables 9, 10, and 11 show the calculated column densities and fractional abundances at $R = 800$ AU for different values of the photodesorption yield. The yield determined for water by Westley et al. (1995), Y_0, has a value of 3.5×10^{-3} molecules per photon. Species shown with asterisks were observed by Dutrey et al. (1997), and the frac-

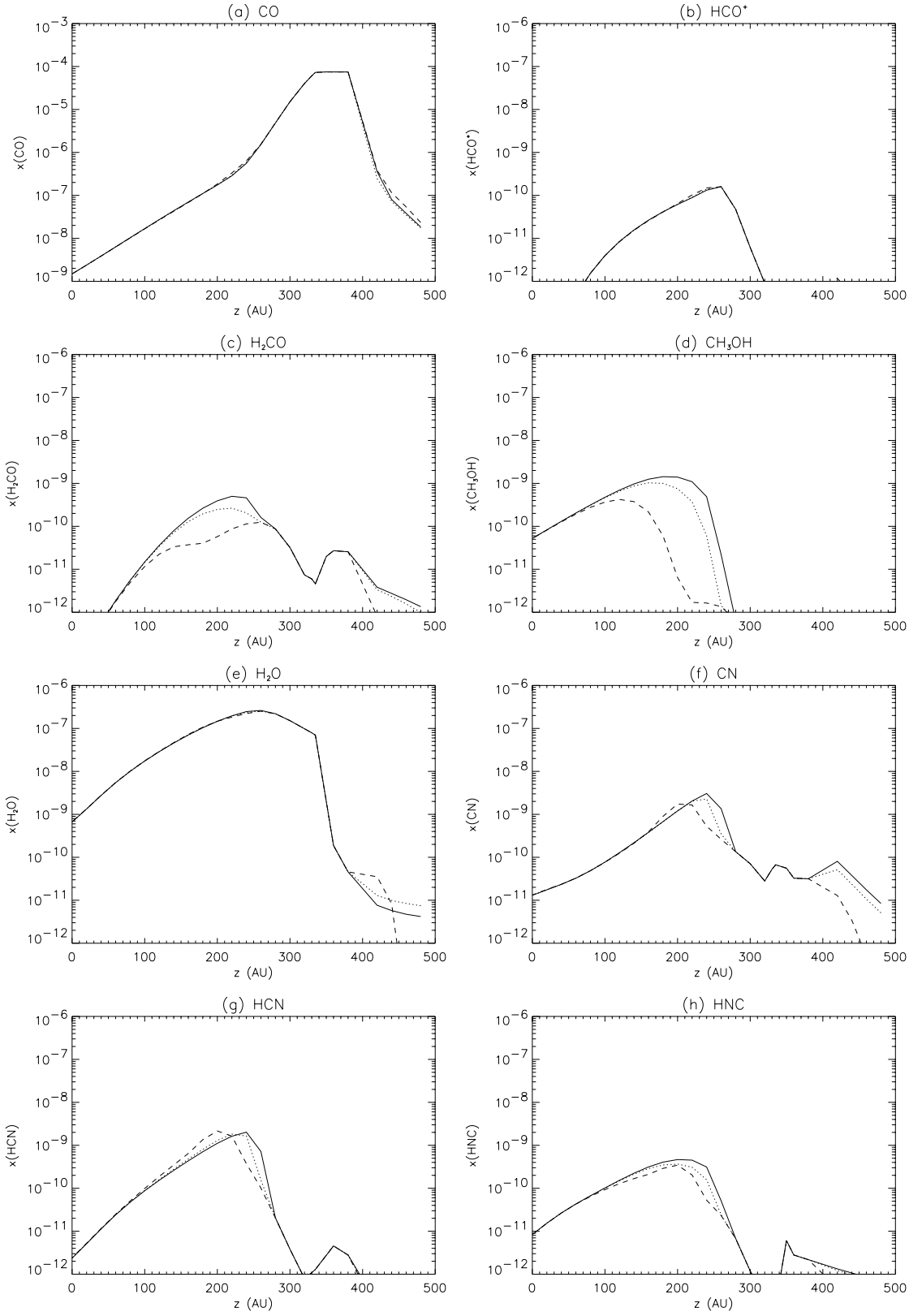

FIG. 4.—Vertical abundance distribution relative to total hydrogen density of several important species in the disk at $R = 800$ AU. The results at three times are shown: 0.5 Myr (*solid lines*), 1 Myr (*dotted lines*), and 5 Myr (*dashed lines*). The abundances of most species can be seen to be constant over the time period displayed here.

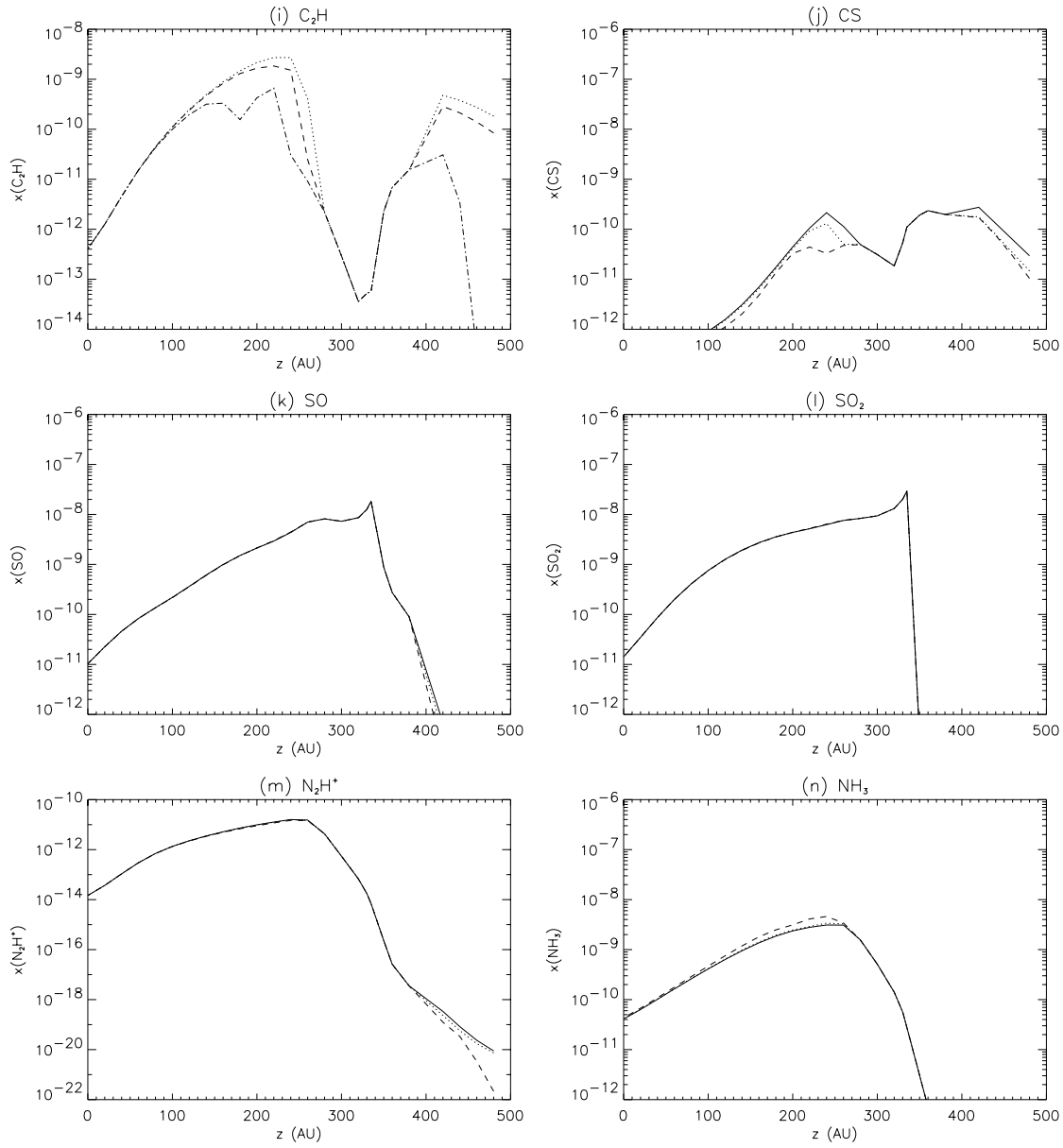

FIG. 4.—*Continued*

tional abundances with asterisks are those which agree with the observations to within a factor of 5. It can be seen that a high photodesorption efficiency ($Y \geq Y_0/3$) is required to account for the observations.

5. COMPARISON WITH OBSERVATIONS

5.1. *DM Tau*

Dutrey et al. (1997) used the IRAM 30 m telescope to make observations of the disk around DM Tau, one of the oldest T Tauri stars in the Taurus region (age $\sim 5 \times 10^6$ yr). Its CO disk has a radius of ~ 800 AU (Guilloteau & Dutrey 1994). Several molecules were observed, and their fractional abundances are given in Table 12. We have compared these to our results at 800 AU and consider good agreement to be within a factor of 5. Tables 7 and 8 give the fractional abundances calculated at 1 and 5 Myr with those species which have been observed shown with asterisks. Abundances which are in good agreement with the observations are also shown with asterisks.

Both times give good agreement for most molecules. The exception is C_2H which is about 15 times underabundant. H_2CO agrees only at 1 Myr, but the other abundances are fit very well at both times. The model is therefore very successful in reproducing the observations of the outer disk.

5.2. *L1157*

A tentative detection of methanol toward the infrared source L1157 was made by Goldsmith et al. (1999). The emission is not resolved and therefore its exact location in the disk cannot be determined, but it appears to be essentially pointlike, in contrast to the more extended continuum emission. If the emission is spread out over the whole of the observed disk, then the fractional abundance of CH_3OH is $\sim 8 \times 10^{-10}$. If the emission is contained within a radius of 100 AU from the central source, then $f(CH_3OH) = 2 \times 10^{-8}$.

In our model the peak fractional abundance of methanol is 10^{-9} at 1000 AU. The calculated abundance is consistent with the observed abundance (if the observed emission

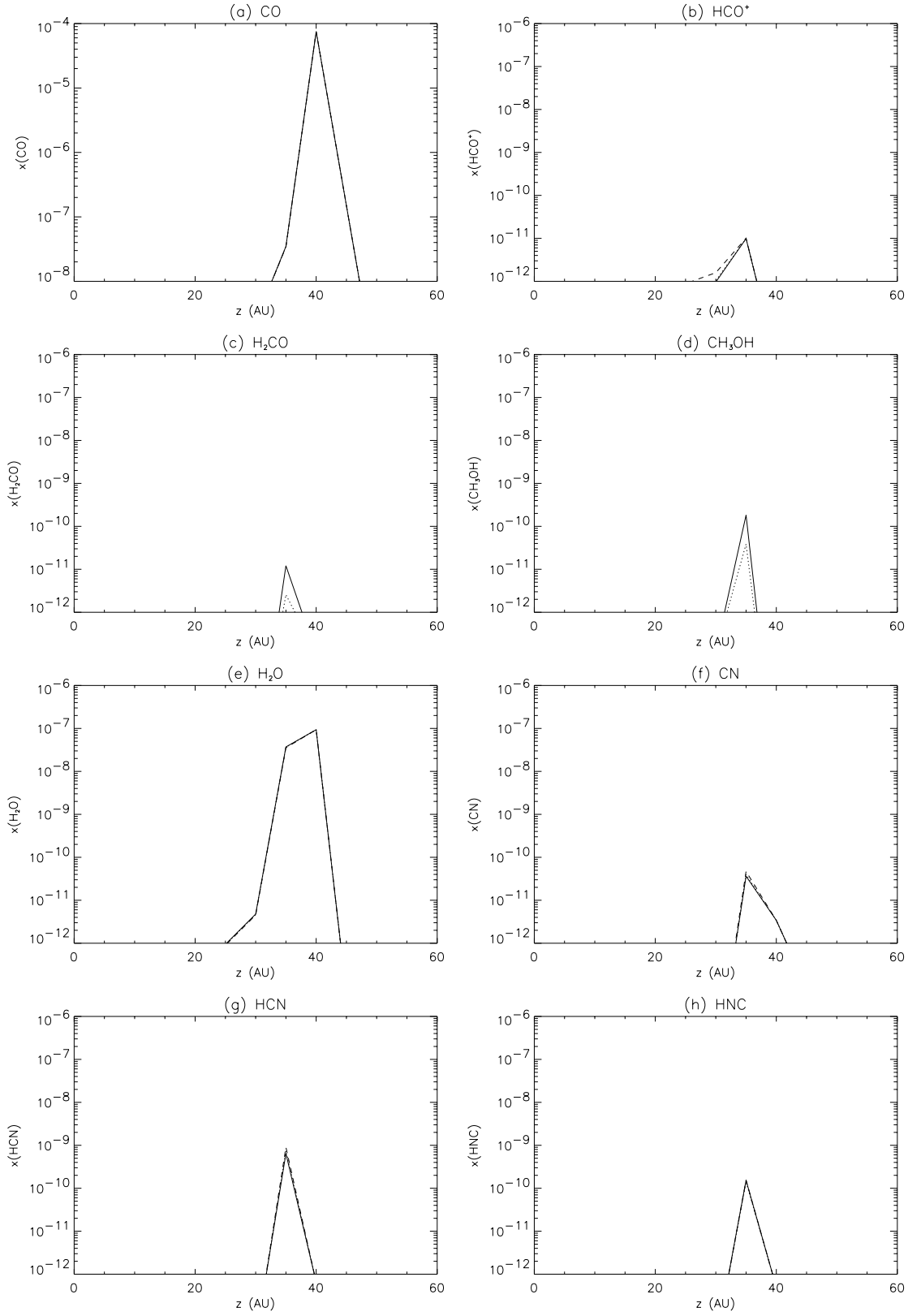

FIG. 5.—As for Fig. 4 but for a radius of 100 AU

comes from the whole of the disk) for $R > 600$ AU. However, at 1000 AU the densities in the layers for which methanol is gaseous might not be sufficiently high to thermalize the observed transition.

Since the continuum appears to be more extended than the methanol emission, it may be more appropriate to compare our results at smaller radii with the observations. At $R < 300$ AU we find very low abundances of methanol,

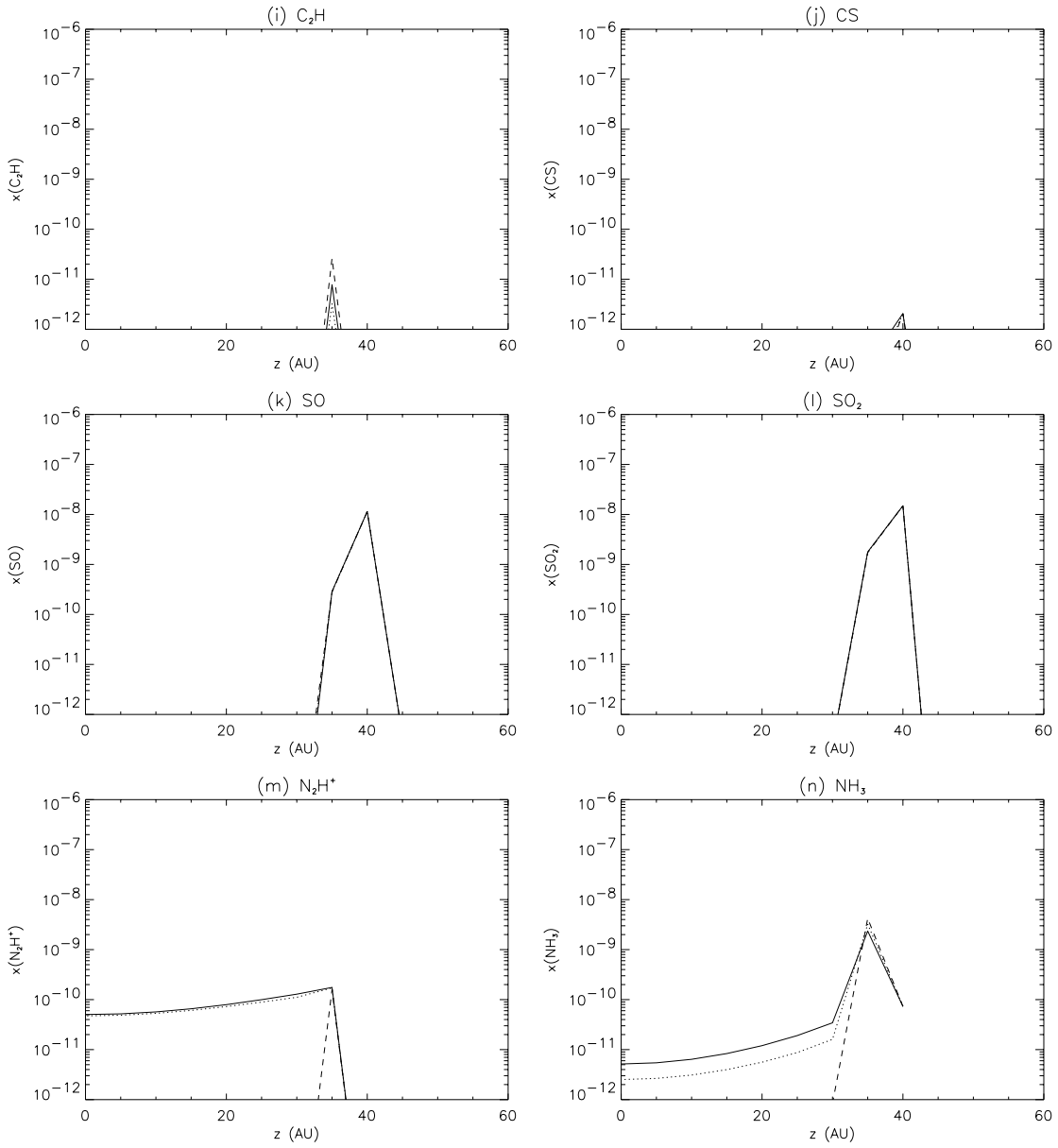

FIG. 5.—*Continued*

since photodesorption is inefficient in this region of the disk and the temperature used in the model is not yet high enough to evaporate the methanol ices. The thermal desorption efficiency depends on the binding energy of the molecule. Two estimates of the binding energy of methanol are found in the literature. In the laboratory Sandford & Allamandola (1993) find a binding energy of 4235 K (the value used in the present work) which means that in our model methanol is only thermally desorbed for $R < 3.3$ AU. Hasegawa & Herbst (1993) use a lower value of 2060 K resulting in thermal desorption within 22 AU. Beam dilution effects mean that very high abundances would be required to account for the observations if the emission were confined to such a small radius. Therefore, the detection of CH_3OH, if it is confirmed to originate close to the star, may indicate that the temperatures in disks are higher than calculated in the CG97 model or that additional desorption processes are acting.

6. CONCLUSIONS

We have presented the results of two-dimensional chemical models of protoplanetary disks. We find that UV radiation is important in driving desorption from grains in the cool regions of the disk below the superheated dust layer described by CG97. The superheated layer itself does not contain molecules since these are quickly dissociated by the intense UV field. The observed emission comes from a layer below the surface where UV photons can still penetrate sufficiently to drive desorption but molecules are shielded to a certain extent from photodestruction. Below this gaseous layer ($A_V^{IS} \geq 4$) molecules are accreted onto icy mantles. If photodesorption can occur at the high rates determined experimentally by Westley et al., then this process can keep even large molecules in the gas. We find good agreement with the observed abundances for photodissociation yields greater than $\sim 10^{-3}$ molecules per photon. Therefore, observations of molecules in disks may

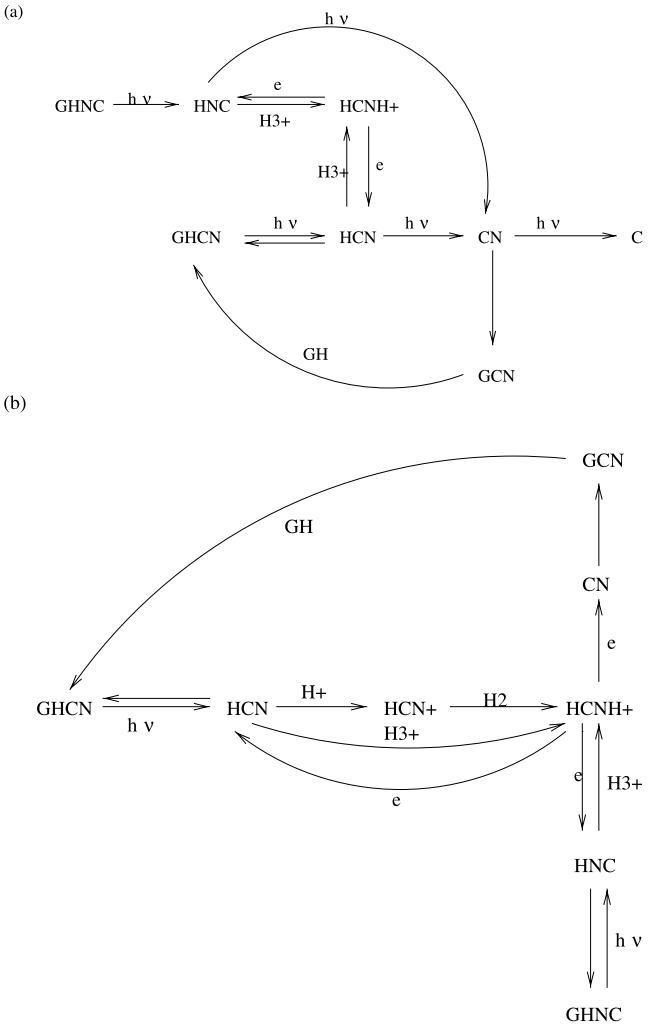

FIG. 6.—Reaction network linking CN, HCN, and HNC at (*a*) $z = 240$ AU and (*b*) $z = 100$ AU. The prefix "G" indicates a molecule in the grain mantle.

TABLE 10

COLUMN DENSITIES AND FRACTIONAL ABUNDANCES (RELATIVE TO H_2) CALCULATED AT 1 Myr AT 800 AU FOR DIFFERENT VALUES OF THE PHOTODESORPTION YIELD, Y

	COLUMN DENSITY				$N(x)/N(H_2)$			
SPECIES	Y_0	$Y_0/3$	$Y_0/10$	$Y_0/50$	Y_0	$Y_0/3$	$Y_0/10$	$Y_0/50$
CO*	6.7(16)	4.4(16)	1.7(16)	2.5(15)	1.9(−5)*	1.3(−5)*	4.9(−6)*	7.3(−7)
H_2CO*	4.8(11)	2.8(11)	1.3(11)	3.5(10)	1.4(−10)*	8.3(−11)	3.9(−11)	1.0(−11)
CH_3OH.....	2.3(12)	1.2(12)	5.6(11)	1.6(11)	6.6(−10)	3.6(−10)	1.6(−10)	4.6(−11)
HCO^+*	1.9(11)	1.0(11)	5.0(10)	1.7(10)	5.6(−11)	2.9(−11)	1.5(−11)	4.8(−12)
N_2H^+*	2.6(10)	1.4(10)	6.3(9)	1.3(9)	7.4(−12)	4.1(−12)	1.8(−12)	3.9(−13)
CN*	2.6(12)	1.8(12)	8.8(11)	1.3(12)	7.4(−10)*	5.1(−10)	2.6(−10)	3.9(−10)
HCN*	2.3(12)	8.5(11)	2.6(11)	1.3(11)	6.6(−10)*	2.5(−10)*	7.4(−11)	3.7(−11)
HNC*	8.2(11)	4.2(11)	1.7(11)	1.0(11)	2.4(−10)*	1.2(−10)*	5.0(−11)*	3.1(−11)
C_2H*	2.8(12)	1.7(12)	7.8(11)	3.6(11)	8.1(−10)	4.9(−10)	2.3(−10)	1.1(−10)
CS*	3.1(11)	1.4(11)	9.2(10)	7.2(10)	9.0(−11)*	4.0(−11)	2.7(−11)	2.1(−11)
SO	1.4(13)	4.5(12)	1.1(12)	1.7(11)	4.1(−9)	1.3(−9)	3.3(−10)	5.0(−11)
SO_2	2.0(13)	7.0(12)	1.8(12)	2.7(11)	5.7(−9)	2.0(−9)	5.3(−10)	7.8(−11)
H_2S	1.8(12)	1.4(12)	3.2(11)	3.1(11)	5.2(−10)	4.1(−10)	9.4(−11)	9.1(−11)
H_2	3.4(21)	3.4(21)	3.4(21)	3.4(21)	1.0	1.0	1.0	1.0

NOTES.—Y_0 is the value of Y taken from Westley et al. 1995. Species observed by Dutrey et al. 1997 are shown with asterisks, and those calculated fractional abundances which are within a factor of 5 of the observed values (or which are consistent with the upper limit in the case of N_2H^+) are also indicated with asterisks. The observed values are given in Table 12. Values are $A(B) = A \times 10^B$.

TABLE 11

COLUMN DENSITIES AND FRACTIONAL ABUNDANCES (RELATIVE TO H_2) CALCULATED AT 5 Myr AT 800 AU FOR DIFFERENT VALUES OF THE PHOTODESORPTION YIELD, Y

	COLUMN DENSITY				$N(x)/N(H_2)$			
SPECIES	Y_0	$Y_0/3$	$Y_0/10$	$Y_0/50$	Y_0	$Y_0/3$	$Y_0/10$	$Y_0/50$
CO*	6.7(16)	4.4(16)	1.7(16)	2.5(15)	2.0(−5)*	1.3(−5)*	5.2(−6)*	7.6(−7)
H_2CO*	2.3(11)	1.4(11)	7.6(10)	2.2(10)	6.8(−11)	4.1(−11)	2.3(−11)	6.8(−12)
CH_3OH.....	8.8(11)	5.9(11)	3.3(11)	1.2(11)	2.7(−10)	1.8(−10)	1.0(−10)	3.5(−11)
HCO^+*	2.0(11)	1.0(11)	5.1(10)	1.6(10)	6.0(−11)	3.1(−11)	1.5(−11)	5.0(−12)
N_2H^+*	2.4(10)	1.3(10)	5.6(9)	9.8(8)	7.4(−12)	3.9(−12)	1.7(−12)	3.0(−13)
CN*	2.2(12)	1.6(12)	1.5(12)	7.0(11)	6.8(−10)*	4.8(−10)	4.5(−10)	2.1(−10)
HCN*	2.5(12)	1.0(12)	5.5(11)	9.7(10)	7.4(−10)*	3.1(−10)*	1.7(−10)*	3.0(−11)
HNC*	6.6(11)	3.5(11)	1.8(11)	7.4(10)	2.0(−10)*	1.1(−10)*	5.3(−11)*	2.2(−11)
C_2H*	8.6(11)	5.1(11)	3.6(11)	1.9(11)	2.6(−10)	1.5(−10)	1.1(−10)	5.8(−11)
CS*	2.6(11)	1.2(11)	8.9(10)	7.3(10)	8.0(−11)*	3.5(−11)	2.7(−11)	2.2(−11)
SO	1.4(13)	4.5(12)	1.1(12)	1.7(11)	4.3(−9)	1.4(−9)	3.4(−10)	5.2(−11)
SO_2	2.0(13)	7.0(12)	1.8(12)	2.7(11)	6.0(−9)	2.1(−9)	5.5(−10)	8.2(−11)
H_2S	1.8(12)	1.4(12)	3.5(11)	3.4(11)	5.5(−10)	4.4(−10)	1.1(−10)	1.0(−10)
H_2	3.3(21)	3.3(21)	3.3(21)	3.3(21)	1.0	1.0	1.0	1.0

NOTES.—Y_0 is the value of Y taken from Westley et al. 1995. Species observed by Dutrey et al. 1997 are shown with asterisks, and those calculated fractional abundances which are within a factor of 5 of the observed values (or which are consistent with the upper limit in the case of N_2H^+) are also indicated with asterisks. The observed values are given in Table 12. Values are $A(B) = A \times 10^B$.

TABLE 12

OBSERVED ABUNDANCES

Species	$f(x)$
CO	1.4(−5)
H_2CO	5.0(−10)
HCO^+	7.4(−10)
CN	3.2(−9)
HCN	5.5(−10)
HNC	2.4(−10)
CS	3.3(−10)
C_2H	1.1(−8)
N_2H^+	<2(−10)

mainly trace the physical and chemical conditions of the surface layers rather than the midplane where most of the mass resides.

Part of this research was carried out while K. W. was a National Research Council Research Associate at the Jet Propulsion Laboratory, California Institute of Technology. This research was conducted at the Jet Propulsion Laboratory, California Institute of Technology under support from the National Aeronautics and Space Administration.

REFERENCES

Aikawa, Y., & Herbst, E. 1999, A&A, 351, 233
Aikawa, Y., Umebayashi, T., Nakano, T., & Miyama, S. M. 1997, ApJ, 486, L51
Bauer, I., Finocchi, F., Duschl, W. J., Gail, H.-P., & Schlöder, J. P. 1997, A&A, 317, 273
Blake, G. A., van Dishoeck, E. F., & Sargent, A. I. 1992, ApJ, 391, L99
Bourdon, E. B., Prince, R. H., & Duley, W. W. 1982, ApJ, 260, 909
Buch, V., & Zhang, Q. 1991, ApJ, 379, 647
Charnley, S. B. 1998, ApJ, 509, L121
Chiang, E. I., & Goldreich, P. 1997, ApJ, 490, 368
Chick, K. M., & Cassen, P. 1997, ApJ, 477, 398
Dutrey, A., Guilloteau, S., & Guélin, M. 1997, A&A, 317, L55
Goldsmith, P., Langer, W. D., & Velusamy, T. 1999, ApJ, 519, L173
Graedel, T. E., Langer, W. D., & Frerking, M. A. 1982, ApJS, 48, 321
Greenberg, L. T. 1973, in Interstellar Dust and Related Topics, ed. J. M. Greenberg & H. C. van de Hulst (Dordrecht: Reidel), 413
Guilloteau, S., & Dutrey, A. 1994, A&A, 291, L23
Hartquist, T. W., & Williams, D. A. 1990, MNRAS, 247, 343
Hasegawa, T. I., & Herbst E. 1993, MNRAS, 261, 83
Hasegawa, T. I., Herbst E., & Leung, C. M. 1992, ApJS, 82, 167
Herbig, G. H., & Goodrich, R. W. 1986, ApJ, 309, 294
Herbst, E. 1993, in Dust and Chemistry in Astronomy, ed. T. J. Millar & D. A. Williams (Bristol: IOP Publ.), 177
Irvine, W. M., Schloerb, F. P., Crovisier, J., Fegley, B., & Mumma, M. J. 2000, in Protostars and Planets IV, ed. V. Mannings, A. P. Boss, & S. S. Russell (Tucson: Univ. Arizona Press), 1159
Langer, W. D., Velusamy, T., & Xie, T. 1996, ApJ, 468, L41
Lee, H.-H., Herbst, E., Pineau des Forêts, G., Roueff, R., & Le Bourlot, J. 1996, A&A, 311, 690
Lee, H.-H., Roueff, E., Pineau des Forêts, G., Shalabiea, O. M., Terzierva, R., & Herbst, E. 1998, A&A, 334, 1047
Leung, C. M., Herbst, E., & Huebner, W. F. 1984, ApJS, 56, 231
Lunine, J. I., Engel, S., Rizk, R., & Horanyi, M. 1991, Icarus, 94, 333
Mezger, P. C., Sievers, A., Zylka, R., Haslam, C. G., Kreysa, R., & Lemke, R. 1992, A&A, 265, 743
Millar, T. J., Farquhar, P. R. A., & Willacy, K. 1997, A&AS, 121, 139
Millar, T. J., & Herbst, E. 1990, A&A, 231, 466
Mundy, L. G., Looney, L. W., & Welch, W. J. 2000, in Protostars and Planets IV, ed. V. Mannings, A. P. Boss, & S. S. Russell (Tucson: Univ. Arizona Press), 355
Pickles, J. B., & Williams, D. A. 1977, Ap&SS, 52, 443
Prasad, S. S., & Tarafdar, S. P. 1983, ApJ, 267, 603
Sandford, S. A., & Allamandola, L. J. 1993, ApJ, 417, 815
Shalabiea, O. M., Caselli, P., & Herbst, E. 1998, ApJ, 502, 652
Sternberg, A., & Dalgarno, A. 1995, ApJS, 99, 565
Tielens, A. G. G. M., & Charnley, S. B. 1997, in Planetary and Interstellar Processes Relevant to the Origins of Life, ed. D. C. B. Whittet (Dordrecht: Kluwer), 23
Tielens, A. G. G. M., & Hagen, W. 1982, A&A, 114, 245
Umebayashi, T., & Nakano, T. 1981, PASJ, 33, 617
Walmsley, C. M., Pineau des Forêts, G., & Flower, D. R. 1999, A&A, 342, 542
Westley, M. S., Baragola, R. A., Johnson, R. E., & Baratta, G. A. 1995, Nature, 373, 405
Willacy, K., Klahr, H. H., Millar, T. J., & Henning, Th. 1998, A&A, 338, 995
Willacy, K., Langer, W. D., & Velusamy, T. 1998, ApJ, 507, L171
Williams, D. A. 1998, in Chemistry and Physics of Molecules and Grains in Space, Faraday Discuss. 109 (London: Royal Soc. Chem.), 1